Inorg. Chem. **2008**, *47*, 6711−6725

General Molecular Mechanics Method for Transition Metal Carboxylates and its Application to the Multiple Coordination Modes in Mono- and Dinuclear Mn(II) Complexes

Robert J. Deeth*

Inorganic Computational Chemistry Group, Department of Chemistry, University of Warwick, Coventry CV4 7AL, U.K.

Received February 19, 2008

A general molecular mechanics method is presented for modeling the symmetric bidentate, asymmetric bidentate, and bridging modes of metal-carboxylates with a single parameter set by using a double-minimum M−O−C angle-bending potential. The method is implemented within the Molecular Operating Environment (MOE) with parameters based on the Merck molecular force field although, with suitable modifications, other MM packages and force fields could easily be used. Parameters for high-spin d^5 manganese(II) bound to carboxylate and water plus amine, pyridyl, imidazolyl, and pyrazolyl donors are developed based on 26 mononuclear and 29 dinuclear crystallographically characterized complexes. The average rmsd for Mn−L distances is 0.08 Å, which is comparable to the experimental uncertainty required to cover multiple binding modes, and the average rmsd in heavy atom positions is around 0.5 Å. In *all* cases, whatever binding mode is reported is also computed to be a stable local minimum. In addition, the structure-based parametrization implicitly captures the energetics and gives the same relative energies of symmetric and asymmetric coordination modes as density functional theory calculations in model and "real" complexes. Molecular dynamics simulations show that carboxylate rotation is favored over "flipping" while a stochastic search algorithm is described for randomly searching conformational space. The model reproduces Mn−Mn distances in dinuclear systems especially accurately, and this feature is employed to illustrate how MM calculations on models for the dimanganese active site of methionine aminopeptidase can help determine some of the details which may be missing from the experimental structure.

Introduction

Carboxylates bind readily to transition metal cations.[1] They are common in coordination chemistry and play a significant role at the active sites of many metalloproteins.[2]

Carboxylates exhibit diverse coordination modes (Figure 1) from monodentate, where the ligand is part of a chelate ring (Figure 1, top left), through symmetrical or asymmetrical bidentate, to bridging via syn and/or anti linkages.

Modeling this diversity computationally is a challenge for force-field (FF) methods, especially for the bidentate modes, since the method should automatically determine the preferred mode as well as "flip", that is, smoothly switch from short−long asymmetric bidentate through symmetric to long−short asymmetric bidentate.

To the author's knowledge, no systematic FF study of metal-carboxylate interactions is available and there are only a few reports involving manganese(II). Riley et al.[3] have used MM2 to study aza macrocylic systems while Beagley et al.[4] also used MM2 for dinuclear Mn salen complexes. Proserpio et al.[5] applied the Universal Force Field (UFF) to peroxido bridged polynuclear Mn complexes as models for photosystem II species. UFF was also employed by Wei et

* To whom correspondence should be addressed. E-mail: r.j.deeth@warwick.ac.uk.

(1) Mehrotra, R. C.; Bohra, R. *Metal Carboxylates*; Academic Press: New York, 1983.
(2) Frausto da Silva, J. J. R.; Williams, R. J. P. *The Biological Chemistry of the Elements: The Inorganic Chemistry of Life.*; Clarendon Press: Oxford, U.K., 1991.
(3) Riley, D. P.; Henke, S. L.; Lennon, P. J.; Aston, K. *Inorg. Chem.* **1999**, *38*, 1908–1917.
(4) Beagley, B.; Edge, N. C.; Jaiboon, N.; James, J. J.; McAuliffe, C. A.; Thorp, M. S.; Watkinson, M.; Whiting, A.; Wright, D. C. *Tetrahedron* **1996**, *52*, 10193–10204.
(5) Proserpio, D. M.; Rappe, A. K.; Gorun, S. M. *Inorg. Chim. Acta* **1993**, *213*, 319–324.

10.1021/ic800313s CCC: $40.75
Published on Web 07/03/2008

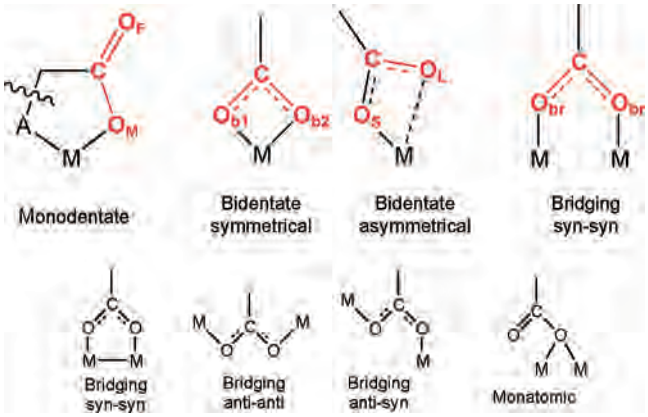

Figure 1. Potential carboxylate binding modes. The modes shown on the top row are considered explicitly although antianti and antisyn bridging modes are within the scope of the parametrization.

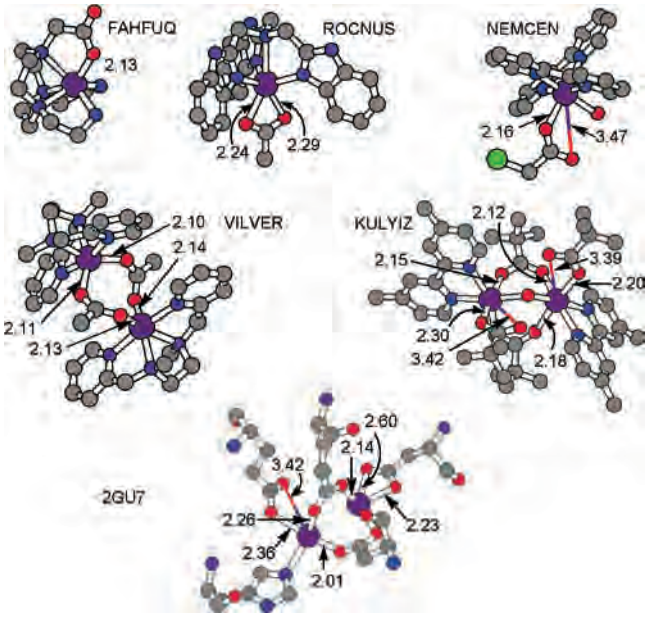

Figure 2. Examples of Mn-carboxylate binding motifs with Cambridge Structural Database refcodes. 2GU7 is the protein databank code for one form of methane aminopeptidase from *Escherichia coli*.[14] Selected Mn−O distances (Å) are indicated by arrows.

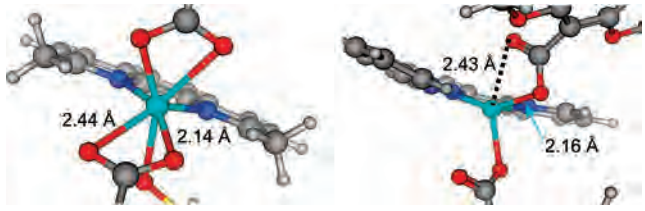

Figure 3. CSD representations of Mn-carboxylate binding. Although the degree of asymmetry is the same, the left-hand structure is encoded as bidentate while the right-hand structure is encoded as monodentate.

al.[6] to study the binding of oxytocin, a complex nonapeptide, to a range of metal centers including Mn(II). The authors favor six-coordinate models which bind the Mn center via amine N, peptide N, and carbonyl oxygen donors.

(6) Wei, H.; Luo, X. M.; Wu, Y. B.; Yao, Y.; Guo, Z. J.; Zhu, L. G. *Dalton Trans.* **2000**, 4196–4200.

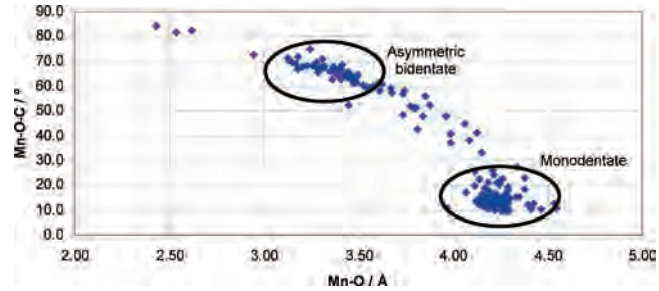

Figure 4. Correlation between the distance from Mn to the further O and the attendant Mn−O−C angle for mononuclear manganese(II)-carboxylato systems.

Table 1. Average Distances and Angles for the Asymmetric Bidentate Mode (see Figure 1) in Mononuclear Mn(II)-Carboxylate Complexes

	MnO_S /Å	MnO_L /Å	MnO_SC /°	MnO_LC /°
value	2.13	3.37	128.0	65.3
std. dev.	0.04	0.24	8.9	5.9

Table 2. Average Distances and Angles for the Monodentate Mode (see Figure 1) in Mononuclear Mn(II)-Carboxylate Complexes

	MnO_M /Å	MnO_F /Å	MnO_MC /°	MnO_FC /°
value	2.18	4.22	123.3	15.2
std. dev.	0.07	0.08	7.5	5.9

Table 3. Average Distances and Angles for the Symmetric Bidentate Mode (see Figure 1) in Mononuclear Mn(II)-Carboxylate Complexes

	MnO /Å	MnOC /°
value	2.30	92.1
std. dev.	0.10	4.8

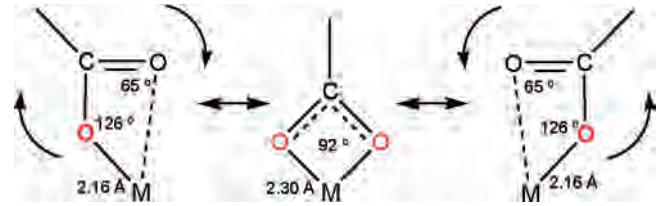

Figure 5. "Flipping" motion of a bound carboxylate including the average structural parameters for bidentate coordination.

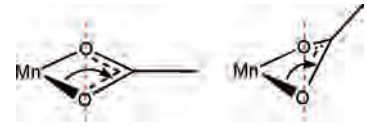

Figure 6. Folding around the O−O vector (red dotted line) decreases the Mn−O−C angle.

Nicolai et al.[7] have carried out methyl group dynamics simulations on $Mn(acetate)_2(H_2O)_4$ based on UFF while Comba et al.[8] deal with several acetato-bispidine complexes, including two Mn(II) species, but focus on the bispidine ligand. Hancock has made extensive use of MM for TM systems and a recent review[9] includes many carboxylate-containing ligands but invariably of the chelating type (monodentate binding as defined in Figure 1).

(7) Nicolai, B.; Kearley, G. J.; Cousson, A.; Paulus, W.; Fillaux, F.; Gentner, F.; Schroder, L.; Watkin, D. *Acta Crystallogr. Sect. B* **2001**, *57*, 36–44.

(8) Comba, P.; Kerscher, M.; Merz, M.; Muller, V.; Pritzkow, H.; Remenyi, R.; Schiek, W.; Xiong, Y. *Chem.—Eur. J.* **2002**, *8*, 5750–5760.

(9) Hancock, R. D.; Melton, D. L.; Harrington, J. M.; McDonald, F. C.; Gephart, R. T.; Boone, L. L.; Jones, S. B.; Dean, N. E.; Whitehead, J. R.; Cockrell, G. M. *Coord. Chem. Rev.* **2007**, *251*, 1678–1689.

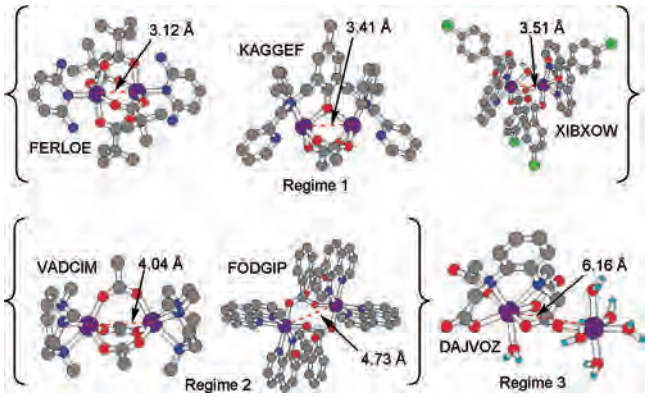

Figure 7. Examples of dinuclear complexes illustrating the three distance regimes, regime 1 (3−3.8 Å), regime 2 (3.8−5 Å), and regime 3 (>5 Å).

These methods require the user to specify (and fix) the binding mode at the start of the calculation and, if asymmetric, to decide *a priori* which M−O bond will be short and which will be long. Moreover, since different parameter sets are used for different coordination modes, direct energy comparisons are impossible because the reference states are different in each case.

This paper describes a solution to these problems. Although applicable to any metal, the one considered here is high-spin d^5 Mn^{2+} which has been chosen for four reasons.

First, high-spin d^5 Mn(II) has no d electronic effects and should therefore be amenable to a conventional MM treatment. Thus, although this work describes a Ligand Field Molecular Mechanics (LFMM)[10] implementation, we do not need any Mn−L angular overlap model (AOM)[11] parameters and so what follows could easily be implemented in any modeling package.

Second, manganese-carboxylate complexes represent an exacting test since they display all the binding modes shown in Figure 1 (examples extracted from the Cambridge Structural Database (CSD)[12] are shown in Figure 2).

Third, Mn(II)-carboxylato moieties are biologically relevant[13] and feature at the active sites of, for example, arginase, Mn-dependent superoxide dismutase,[2] and methionine aminopeptidase (MetAP). The latter contains symmetrical bidentate, asymmetrical bidentate, and bridging carboxylate ligands (Figure 2).[14]

Finally, computational approaches to manganese-containing systems are dominated by QM and QM/MM methods as in, for example, some recent work on generic Mn_2 systems,[15] photosystem II,[16,17] and MetAP[18] plus the ab initio molecular dynamics study of arginase.[19] Compared to MM, all these techniques are more or less compute intensive. This paper explores to what extent "pure" molecular mechanics might be a viable alternative for manganese complexes in general and Mn-carboxylato interactions in particular.

Computational Details

All the MM calculations were carried out using DommiMOE,[20] our extended version of the Molecular Operating Environment (MOE).[21] DommiMOE is available from the author on request and, aside from a modest handling fee, there are no additional licensing issues beyond those for MOE itself. MOE uses a generic form for the potential energy (see Supporting Information) which can accommodate a range of particular force fields. The Merck molecular force field MMFF94x has been used here where the 'x' refers to an extension of MMFF94s[22,23] which ensures that conjugated nitrogens are planar.

A "purely MOE" version has also been developed by setting the L−Mn−L angle bending force constants to zero, adding new scientific vector language (SVL) code for explicit ligand−ligand repulsions ($1/d^6$ dependence), and fitting the Morse function curves to MOE's native quartic expansion out to about 3.5 Å. Optimized geometries from "conventional" MOE and LFMM are essentially identical, and the relevant SVL scripts for energy minimization are available from the author upon request.

Molecular dynamics (MD) simulations used the Nosé−Poincaré−Anderson (NPA) method implemented in MOE2006.[24,25] The constant number of particles, volume, and temperature (NVT) ensemble with $T = 300$ K was used. The complex was immersed in a 10 Å thick layer of water molecules, and the whole system minimized to a gradient norm of less than 0.01 prior to starting the MD run.

Density functional theory (DFT) calculations used the 2006 version of the Amsterdam density functional (ADF) program.[26] Geometry optimizations employed the spin-unrestricted Becke−Perdew (BP86) functional[27,28] with basis sets of triple-ζ plus polarization (TZP) quality on the metal and double-ζ plus polarization (DZP) on all other atoms together with the frozen core approximation[29] (1s−2p on Mn and Cl, 1s on C, N, and O). Single-point energy

(10) Deeth, R. J. *Coord. Chem. Rev.* **2001**, *212*, 11–34.
(11) Schaeffer, C. E.; Jorgensen, C. K. *Mol. Phys.* **1965**, *9*, 401.
(12) Allen, F. H. *Acta Crystallogr.* **2002**, *B58*, 380–388.
(14) Ye, Q. Z.; Xie, S. X.; Ma, Z. Q.; Huang, M.; Hanzlik, R. P. *Proc. Nat. Acad. Sci. U.S.A.* **2006**, *103*, 9470–9475.
(13) de Boer, J. W.; Browne, W. R.; Feringa, B. L.; Hage, R. *C. R. Chim.* **2007**, *10*, 341–354.
(15) Liu, S. B.; Perera, L.; Pedersen, L. G. *Mol. Phys.* **2007**, *105*, 2893–2898.
(16) Sproviero, E. M.; Gascon, J. A.; McEvoy, J. P.; Brudvig, G. W.; Batista, V. S. *J. Chem. Theory Comput.* **2006**, *2*, 1119–1134.
(17) Siegbahn, P. E. M. *Curr. Opin. Chem. Biol.* **2002**, *6*, 227–235.
(18) Leopoldini, M.; Russo, N.; Toscano, M. *J. Am. Chem. Soc.* **2007**, *129*, 7776–7784.
(19) Ivanov, I.; Klein, M. L. *Proteins: Struct., Funct., Genet.* **2004**, *54*, 1–7.
(20) Deeth, R. J.; Fey, N.; Williams-Hubbard, B. J. *J. Comput. Chem.* **2005**, *26*, 123–130.
(21) *MOE Molecular Operating Environment, 2006.06*; Chemical Computing Group, Montreal: Montreal, 2006.
(22) Halgren, T. A. *J. Comput. Chem.* **1999**, *20*, 720–729.
(23) Halgren, T. A. *J. Comput. Chem.* **1999**, *20*, 730–744.
(24) Sturgeon, J. B.; Laird, B. B. *Symplectic Algorithm for Constant Pressure Molecular Dynamics Using a Nosé-Poincaré Thermostat.*; Technical Paper; University of Kansas: Lawrence, KS, 2002.
(25) Bond, S. D.; Benedict, J. L.; Laird, B. B. *J. Comp. Phys.* **1999**, *151*, 114–134.
(26) Baerends, E. J.; Bérces, A.; Bo, C.; Boerrigter, P. M.; Cavallo, L.; Deng, L.; Dickson, R. M.; Ellis, D. E.; Fan, L.; Fischer, T. H.; Fonseca Guerra, C.; van Gisbergen, S. J. A.; Groeneveld, J. A.; Gritsenko, O. V.; Harris, F. E.; van den Hoek, P.; Jacobsen, H.; van Kessel, G.; Kootstra, F.; van Lenthe, E.; Osinga, V. P.; Philipsen, P. H. T.; Post, D.; Pye, C. C.; Ravenek, W.; Ros, P.; Schipper, P. R. T.; Schreckenbach, G.; Snijders, J. G.; Sola, M.; Swerhone, D.; te Velde, G.; Vernooijs, P.; Versluis, L.; Visser, O.; van Wezenbeek, E.; Wiesenekker, G.; Wolff, S. K.; Woo, T. K.; Ziegler, T. *ADF 2006.01, Scientific Computing and Modelling NV*; Free University, Amsterdam: Amsterdam, 2006.
(27) Becke, A. D. *Phys. Rev. A* **1988**, *38*, 3098–3100.
(28) Perdew, J. P. *Phys. Rev. B: Condens. Matter* **1986**, *33*, 8822–8824.
(29) Baerends, E. J.; Ellis, D. E.; Ros, P. *Theoret. Chim. Acta* **1972**, *27*, 339.

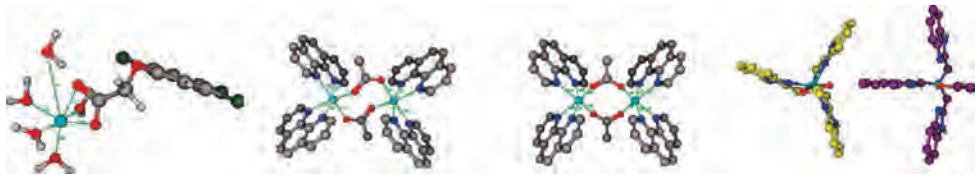

Figure 8. Structures from "disconnected" calculations. Far left: after a few ps of MD, water ligands dissociate from the complex. Dinuclear complexes: the left-hand species shows the starting X-ray coordinates which clearly shows asymmetry in the bridge which is lost upon minimizing (right-hand example). Tripod complexes: the starting X-ray structure (yellow carbons) loses its 3-fold symmetry upon optimization (purple carbons).

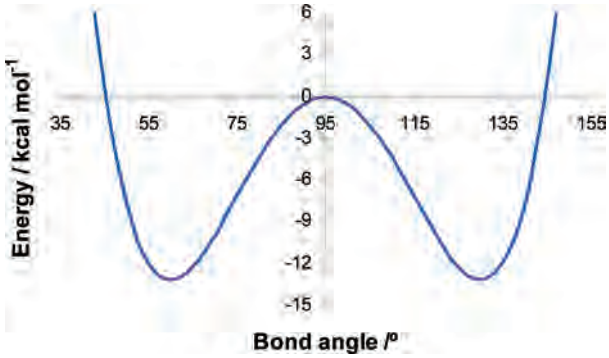

Figure 9. Sketch of angle bending potential of the form $E_\theta = k_2(\theta - \theta_0)^2 + k_4(\theta - \theta_0)^4$ with $k_2 = -70$ kcal mol^{-1} radian^{-2} and $k_4 = 93$ kcal mol^{-1} radian^{-4}.

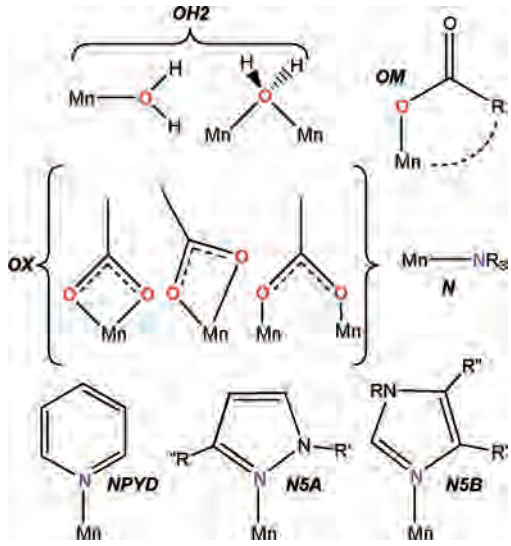

Figure 10. Binding modes and associated MMFF atom-type labels (italic) for the ligands considered here.

Table 4. Ligand Types, MMFF Donor-Atom Labels, and Bond Charge Increment Values for Mn Complexes

ligand	MMFF atom type	bci
water	OH2	0.15
monodentate RCO_2	OM	0.10
bidentate/ bridging RCO_2	OX	0.08
amine	N	0.18
pyridyl	NPYD	0.20
pyrazolyl	N5A	0.20
imidazolyl	N5B	0.20

calculations used TZP basis sets throughout and a variety of functionals as described in the text. Self-consistent field (SCF) convergence was aided by strongly damping the SCF mixing parameter (0.01 compared to the default maximum of 0.3) and applying a level shift of 0.3 au to the virtual orbitals. Default SCF and geometry optimization convergence criteria were used except for the latter where the Cartesian displacement convergence threshold was increased from 0.01 to 0.02 Å. Spin contamination was negligible as judged by the calculated expectation value of $\langle S^2 \rangle$ which never deviated significantly from the ideal value.

Table 5. Morse and Ligand−Ligand Repulsion Parameters[a]

MMFF ligand type	r_0/Å	D/ kcal mol^{-1}	α	A_{LL}/kcal mol^{-1} Å^6
OH2	2.15	50.7	1.6	4500
OM	2.12	50.7	1.2	5000
OX	2.15	50.7	1.6	6000
NPYD	2.05	60.0	1.00	5000
N	2.25	58.0	1.00	2800
N5A	2.00	60.0	0.80	4500
N5B	1.90	60.0	1.00	5500

[a] D = well depth, r_0, = reference bond length, α = curvature parameter, A_{LL} = ligand−ligand repulsion parameter for a d^{-6}-dependent term where d is the donor atom−donor atom distance.

All Cambridge structural database (CSD) searches were carried out via the EPSRC Chemical Database Service.[30] CSD refcodes and full bibliographic and chemical data are given in the Supporting Information (Tables S1 through S4).

Results and Discussion

The small number of previous MM studies on manganese carboxylates perhaps reflects the difficulties of modeling transition metal systems in general and metal-carboxylate interactions in particular. Our response to the first issue has been to develop a new valence FF approach specifically for TM systems called ligand field molecular mechanics (LFMM).[10] The implementation of LFMM within MOE[20] extends the existing FFs to include metal centers and places metal ions on the same footing as any other atom type. However, because the ligand field stabilization energy is zero for high-spin d^5 systems, the ligand field part of LFMM is redundant here. Thus, any "conventional" MM code, including the unextended version of MOE or perhaps more sophisticated MM methods like the polarizable FF in SIBFA-LF[31] or Goddard's ReaxFF[32] schemes, could be used once the modifications and additions described below have been implemented.

Many types of data could be used to develop the FF parameters. For example, Norrby employs structural data, molecular energies and even Hessian matrix elements to develop extremely accurate, specialized force field for modeling transition states for particular reactions.[33] At a more

(30) Fletcher, D. A.; McMeeking, R. F.; Parkin, D. *J. Chem. Inf. Comput. Sci.* **1996**, *36*, 746–749.
(31) Piquemal, J. P.; Williams-Hubbard, B.; Fey, N.; Deeth, R. J.; Gresh, N.; Giessner-Prettre, C. *J. Comput. Chem.* **2003**, *24*, 1963–1970.
(32) Nielson, K. D.; van Duin, A. C. T.; Oxgaard, J.; Deng, W. Q.; Goddard, W. A. *J. Phys. Chem. A* **2005**, *109*, 493–499.
(33) Norrby, P. O.; Brandt, P. *Coord. Chem. Rev.* **2001**, *212*, 79–109.

Table 6. Comparison of Calculated and X-ray Data for Mononuclear Mn(II) Complexes

No./Refcode	Mn-L Bond length differences (LFMM – X-ray) / Å							Δr [a]	rmsd [b]
1 ADEHIB	-0.02	-0.14	0.03	0.00	0.04	0.02	0.00	0.06	1.04
2 BIZYEO	-0.02	-0.03	0.08	0.02	-0.50	-0.03	0.02	0.19	1.58
3 DEFROW	0.05	-0.02	0.10	0.07	0.03	-0.23		0.11	0.37
4 DEVLIA	0.00	0.09	-0.04	0.14	-0.36	0.06		0.16	0.37
5 FAHFUQ	0.02	0.00	-0.06	-0.01	-0.08	-0.04		0.04	0.13
6 FODGOV	0.04	0.08	0.05	0.00	-0.02	0.08	-0.07	0.06	0.43
7 GAMFIK	0.00	-0.13	0.05	0.06	0.02	0.02	-0.02	0.06	0.55
8 HAYSOQ	-0.04	-0.03	-0.07	0.04	0.07	0.15		0.08	0.41
9 HAZVAF	-0.13	0.00	0.05	0.01	0.08	0.09	-0.08	0.08	0.14
10 HULXER	0.00	0.01	-0.01	-0.12	0.02	0.05	0.03	0.05	0.43
11 LOYBIK	-0.09	0.03	0.03	0.03	0.00	0.04	0.19	0.08	0.57
12 NAMKIW	0.03	0.00	-0.19	-0.02	0.01	-0.05	0.06	0.08	1.31
13 NEMCEN	-0.01	0.00	0.01	-0.11	0.04	0.04	-0.02	0.05	0.54
14 NIPHAV	0.02	-0.09	0.02	0.00	-0.02	0.06	0.01	0.04	0.56
15 OFEFEK	-0.04	0.02	0.11	0.01	0.04	0.01	0.12	0.07	0.59
16 QUSVOP	0.04	-0.03	0.04	-0.03	0.05	0.11	-0.24	0.11	0.27
17 ROCNUS	-0.06	0.07	-0.05	0.05	-0.08	0.06		0.06	0.24
18 SAFQEV	0.01	0.08	-0.02	0.02	-0.12	-0.02		0.06	0.57
19 SUSXAF	0.06	-0.35	-0.06	0.03	0.09	0.08		0.15	0.31
20 UDAMAO	0.04	-0.11	-0.04	0.01	0.00	0.02	0.03	0.05	0.40
21 VEGJEX	-0.02	-0.02	0.05	0.10	-0.10	0.08		0.07	0.30
22 WAMNUU	0.01	-0.03	0.02	0.06	-0.06	0.04	-0.02	0.04	0.40
23 XAFBEM	0.03	-0.01	0.02	0.04	0.07	-0.17	-0.03	0.07	0.34
24 XOGWUL01	-0.04	-0.01	0.04	0.01	0.07	0.00	-0.11	0.06	0.65
25 XUQBIU	0.15	0.10	0.05	0.00	-0.04	-0.21	0.02	0.11	0.23
26 XUXFUR	0.03	0.06	0.05	-0.07	0.00	-0.08	0.01	0.05	0.80
								Av. 0.08	Av. 0.52
Color code	OX	OM1	OH2	N	NPYD	NSA	NSB		

[a] Rmsd for all bonds in complex (Å). [b] Heavy-atom superposition rmsd (Å).

general level, Allured et al.[34] used three approaches to parametrize the SHAPES FF: normal coordinate analysis, ab initio calculations, and structure-based optimization. All three methods gave similar results. Previous LFMM studies have relied on a structure-based FF parametrization,[35–38] often mixing experimental and calculated data. In the case of the Jahn−Teller effect in six-coordinate Cu(II) systems, this allowed us to model quite subtle features of the potential energy surface.[36] Structure-based FF optimization is simple to implement and appears capable of good accuracy, at least with respect to molecular structures and conformational energies.

Mononuclear Structures. The Cambridge Structural Database (CSD) is used both to establish the basic features of Mn-carboxylato interactions and provide a suitable training set. A CSD search for mono- and bidentate mononuclear Mn(II) carboxylates revealed 143 unique structures. The CSD refcodes and relevant bibliographic data are collected in the Supporting Information (Tables S1 and S3).

Although the CSD search specified explicit mono- and bidentate moieties as defined in Figure 1, there are some ambiguities in connectivity searching. For example, (2,9-dimethyl-1,10-phenanthroline)-(dimethyl sulfoxide)-bis(indole-2-carboxylato)-manganese(II) (IJOWEJ) (Figure 3, left) and bis(2,6-dimethoxybenzoato-O)-(2,2′:6,6′-terpyridine)-manganese(II) (LOSVEU) (Figure 3, right) have the same asymmetry but IJOWEJ is coded as bidentate while LOSVEU is coded monodentate.

However, as shown in Figure 4, the Mn−O−C angles clearly separate monodentate coordination, in the sense shown in Figure 1, from the asymmetric bidentate mode.

Taking the structures with long Mn−O distances of less than 3.75 Å as examples of asymmetric coordination, the averages and standard deviations for the short Mn−O bond length (MnO_S), long Mn−O contact (MnO_L) and the respective Mn−O−C angles at O_S and O_L are given in Table 1. The relevant averages for monodentate and symmetric bidentate ligands are in Tables 2 and 3, respectively.

Within the uncertainties shown in Tables 1 and 2, the geometry around the shorter Mn−O bond in both monodentate and asymmetric bidentate is about the same. To span the range from Mn−O_S minus one standard deviation (2.13 − 0.04 = 2.09 Å) to Mn−O_M plus one standard deviation (2.18 + 0.07 = 2.25 Å), the mean Mn−O distance needs to be about 2.17 ± 0.08 Å while the Mn−O−C angle is about 126 ± 10 °. Symmetric bidentate coordination results in both a longer Mn−O bond of 2.30 ± 0.1 Å and Mn−O−C angles of 92 ± 5 °.

The uncertainty needed to span multiple binding modes unsurprisingly tends to be larger than that for any individual mode. The consequence for MM is that requiring a single parameter set to describe multiple binding modes is also likely to lead to larger errors. No doubt, more accurate structures could be obtained with independent parameters for each binding mode but we would then loose both the

(34) Allured, V. S.; Kelly, C. M.; Landis, C. R. *J. Am. Chem. Soc.* **1991**, *113*, 1–12.
(35) Deeth, R. J. *Inorg. Chem.* **2007**, *46*, 4492–4503.
(36) Deeth, R. J.; Hearnshaw, L. J. A. *Dalton Trans.* **2006**, 1092–1100.
(37) Deeth, R. J. *Chem. Commun.* **2006**, 2551–2553.
(38) Deeth, R. J.; Hearnshaw, L. J. A. *Dalton Trans.* **2005**, 3638–3645.

Table 7. Comparison of MM and X-ray Data for Dinuclear Mn(II) Complexes

No./Refcode	Mn-L bond length differences: LFMM - X-ray/ Å							Δr[a]	rmsd[b]	Δd(M-M)[c]
27 ABIDAR	-0.01	0.02	0.11	-0.01	0.13	0.03		0.07	0.30	0.04
	0.11	-0.01	-0.01	0.03	0.13	0.02				
28 ABIDEV	0.11	0.12	0.00	0.03	0.02	0.01		0.07	0.34	-0.03
	0.01	0.02	0.03	0.00	0.12	-0.11				
29 AGUJER	-0.02	-0.05	0.11	-0.01	-0.01	0.11		0.07	0.38	0.10
	0.11	-0.01	-0.02	0.11	-0.05	-0.01				
30 DAJVOZ[d]	0.07	0.04	0.11	-0.03	0.09	0.04		0.07	0.24	0.17
	-0.03	0.05	0.01	0.01	0.13	0.06	-0.05			
31 DEMJUB	0.14	0.13	-0.04	-0.01	0.03	0.01		0.08	0.89	0.12
	0.13	0.14	-0.04	-0.01	0.03	0.01				
32 FERLOE01	0.04	0.09	0.21	0.14	-0.07			0.12	0.74	0.07
	0.04	0.09	-0.07	0.21	0.14					
33 FODGIP	0.10	0.11	0.01	0.02	-0.01	0.01		0.06	0.30	0.02
	0.10	0.11	-0.01	0.01	0.02	0.01				
34 HOZPER	-0.01	0.00	0.14	0.16	0.07	0.02		0.09	0.58	-0.04
	0.00	-0.01	0.02	0.14	0.16	0.07				
35 IDERIS	0.12	0.02	0.10	0.02	0.01	0.00		0.07	0.39	0.10
	0.03	0.02	0.12	0.02	0.06	0.10				
36 IREVUW	0.00	0.14	0.12	0.05	0.05	0.02		0.09	0.20	0.12
	0.05	0.14	0.02	0.12	0.05	0.06				
37 JAXNAY	0.09	-0.15	-0.09	0.16	0.02	-0.05		0.11	0.98	0.39
	-0.05	0.16	0.09	-0.15	0.02	-0.08				
38 KULYIZ	0.14	-0.08	0.11	0.03	0.02	0.02	-0.03	0.07	0.76	-0.01
	0.06	0.01	0.01	0.08	0.01	0.12	-0.05			
39 KULYOF	0.10	0.01	0.09	0.08	-0.07	-0.03	0.03	0.07	0.42	-0.08
	0.08	0.04	0.00	0.11	-0.00	0.09	0.10			
40 MAVMOM01	0.10	0.02	-0.03	0.00	0.00	0.14		0.07	0.18	0.26
	0.00	0.02	0.00	-0.03	0.14	0.10				
41 NEMCAJ	0.15	0.03	-0.01	0.13	-0.01	0.00		0.08	0.59	0.29
	0.03	0.13	-0.01	-0.01	0.00	0.15				
42 NEQPEF	0.17	0.07	0.14	0.02	0.09	0.03		0.10	0.38	-0.10
	0.10	0.08	0.12	0.03	0.13	0.13				
43 NIMNUS	0.10	0.04	-0.09	0.05	0.15	0.10	0.09	0.09	0.59	-0.18
	-0.09	0.04	0.15	0.10	0.09	0.05	0.10			
44 NIMPAA	0.06	0.12	0.14	0.04	0.12	0.03	-0.06	0.09	0.99	-0.15
	0.12	0.03	0.06	0.12	0.13	0.04	-0.06			
45 OGOZEP	0.10	0.00	0.12	0.03	0.01	-0.06		0.07	0.61	0.26
	0.12	0.04	0.00	-0.06	0.10	0.01				
46 PIFVUV	0.01	0.08	0.14	0.04	0.04	-0.02		0.07	0.33	0.16
	-0.02	0.01	0.04	0.04	0.14	0.08				
47 QANCIS	0.11	0.17	-0.21	0.05	0.01	-0.03		0.16	0.59	-0.01
	0.09	-0.41	0.19	-0.03	0.04	0.04				
48 QEMRUW	-0.01	0.04	0.01	0.11	0.02	0.12		0.07	0.22	0.14
	0.02	0.04	-0.01	0.01	0.11	0.11				
49 QERZOD	-0.11	-0.04	0.08	0.14	0.12	0.13		0.11	0.73	0.11
	0.12	0.08	0.14	-0.04	0.13	-0.11				
50 VADCIM	0.07	0.04	0.06	0.02	0.10	0.09		0.07	0.32	-0.26
	0.00	0.08	0.11	0.02	0.13	0.04				
51 VILVER	0.07	0.02	0.04	0.03	0.04	0.08		0.06	0.13	-0.07
	0.10	0.00	0.06	0.00	0.11	0.05				
52 XESVOH	0.05	-0.06	0.12	0.07	-0.01	0.06		0.07	0.36	0.11
	0.07	0.12	-0.01	0.05	0.06	-0.06				
53 XEVGAG	0.01	0.14	-0.23	0.08	0.14	0.12		0.11	0.84	-0.18
	0.05	0.10	-0.03	0.02	0.12	0.12				
54 YAYWOL	-0.02	0.15	-0.11	0.01	0.03	0.16		0.10	0.41	0.39
	0.03	0.15	0.16	-0.11	-0.02	0.01				
55 ZARZEX	0.01	0.08	-0.01	0.12	0.12			0.10	0.94	0.15
	0.10	0.00	0.20	0.14	0.00					
								Av. 0.09	Av. 0.51	Av. S 0.07[e] Av. U 0.14[f]
Color code	OX	OM	OH2	N	NPYD	NSA				

[a] Rmsd for all bonds in complex (Å). [b] Heavy-atom superposition rmsd (Å). [c] Difference between LFMM and X-ray Mn−Mn distances (Å). [d] Solvated LFMM calculation (see text and Figure 17 for discussion). [e] Signed average. [f] Unsigned average.

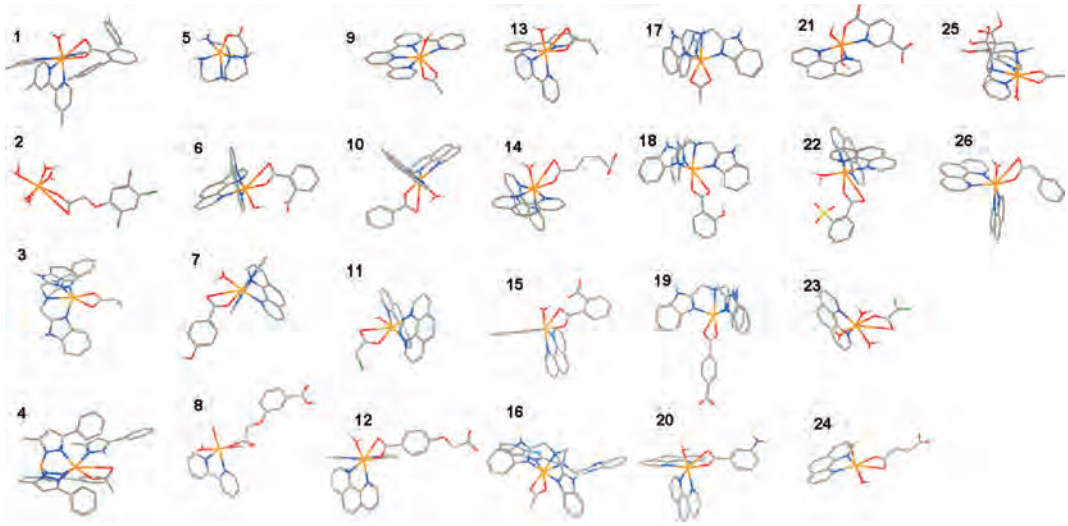

Figure 11. Line figures of mononuclear Mn(II) complexes generated from the X-ray structures. Numbering scheme as per Table 6.

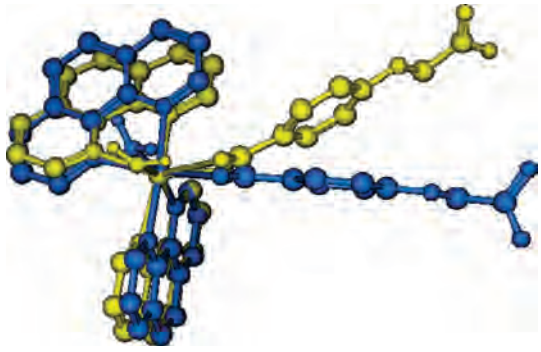

Figure 12. Overlay of X-ray (yellow) and calculated (blue) structures of NAMKIW.

ability to make energetic comparisons plus any smooth switch or "flip" between asymmetric and symmetric modes (Figure 5). These features require a single set of parameters.

The experimental data reveal examples from asymmetric to symmetric bidentate suggesting perhaps that flipping may be relatively facile. However, symmetric bidentate coordination is often associated with an overall lower coordination number. Mn(II) complexes tend to have six short bonds disposed more-or-less octahedrally. If other ligands provide five of those contacts, the carboxylate provides one stronger interaction and thus tends to be asymmetric bidentate whereas if the other ligands provide only four contacts, the carboxylate binds symmetrically to provide two strong interactions.

Dinuclear Structures. Forty-six unique dimanganese complexes with 74 bridging carboxylate groups were located in the CSD (refcodes and bibliographic information in Supporting Information, Tables S2 and S4). The mean Mn−O bond length is 2.11 ± 0.04 Å and the mean Mn−O−C angle is 134 ± 9 °, both of which are within one standard deviation of the nonbridging-modes value. This suggests that a single set of FF parameters should suffice for bridging modes, as well as monodentate and asymmetric bidentate modes. However, for bidentate coordination, the metal usually lies in the carboxylate plane (the Mn−O−C−O dihedral angles equal zero) while when bridging, this is often not the case (the Mn−O−C−O dihedrals are nonzero). This difference requires context-sensitive torsion parameters. The Mn−O−C−O tetrad is assigned a torsional term which minimizes at 0 and 180 ° with a force constant of 12 if the tetrad is part of a 4-membered ring (i.e., a bidentate carboxylate) or 1.5 otherwise (i.e., monodentate or bridging). The larger force constant for bidentate coordination is required to prevent the carboxylate group from "folding" about the O···O vector (Figure 6) in an attempt to get both Mn−O−C angles close to the 58 ° minimum in the angle-bend potential (Figure 9).

Another interesting feature of the dinuclear systems is the Mn−Mn distance which here ranges from 3.06 to 6.26 Å divided roughly into three regimes (Figure 7). Short metal−metal contacts (regime 1 from ∼ 3 to 3.8 Å) are associated with complexes containing four bridging carboxylates {e.g., tetrakis(μ^2-pivalato-O,O′)-bis(2,6-diaminopyridine)-dimanganese(II), (FERLOE)} or two bridging RCO_2 groups plus an additional single-atom bridge like phenoxide {e.g., bis(μ^2-acetato)-(μ^2-2,6-bis(bis(2-pyridylmethyl)aminomethyl)-4-methylphenoxo)-dimanganese(II), (KAGGEF)} or water {e.g., (μ^2-aqua)-bis(μ^2-4-chlorobenzoato-O,O′)-bis((4-chlorobenzoato-O)-(1,10-phenanthroline)-manganese(II)), (XIBXOW)}. The latter gives distances at the top end of the regime but in either case, the geometrical requirements of three or four bridging groups effectively ensures a syn-syn mode for the carboxylates.

In regime 2 (about 3.8 to 5 Å) the only bridging ligands are carboxylates. Three syn-syn bridges {e.g., tris(μ^2-acetato-O,O′)-bis(1,4,7-trimethyl-1,4,7-triazacyclononane-N,N′,N″)-dimanganese(II), (VADCIM) } give a shorter Mn−Mn separation than two syn-anti bridges {e.g., bis((μ^2-hydrogen phthalato-O,O′)-bis(1,10-phenanthroline)-manganese(II)), (FODGIP)}. Beyond 5 Å (regime 3), there is just a single anti-anti bridge with a second Mn complex "hanging off" to one side {e.g., 1,1,1,1,1,2-hexaaqua-(μ^2-o-phenylenediamine-tetra-acetato-O^1:N,N',O^2,O^3,O^4,O^5)-dimanganese(II), (DAJVOZ)}.

Angular Potential. Most if not all MM packages can treat metals as isolated spherical charges. This has the advantage

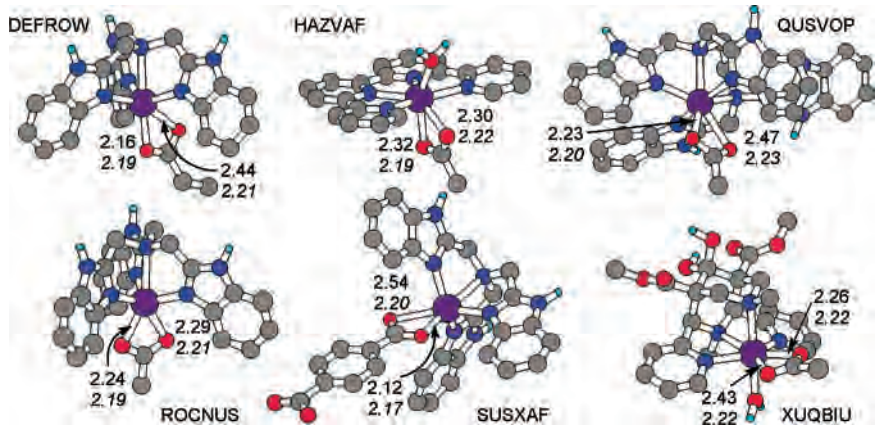

Figure 13. Symmetric mode monodentate complexes with experimental (normal text) and calculated (italics) Mn−O distances. Nonpolar hydrogens have been removed for clarity.

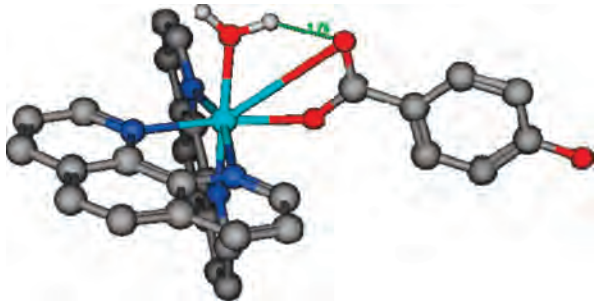

Figure 14. Left: intramolecular H-bond between long Mn−O(carboxylate) and adjacent water ligand in GAMFIK encourage asymmetric bidentate binding. The H−O separation (Å) is shown in green (1.76 Å).

of avoiding further parameter development but does not work well for Mn(II) species. Several examples are shown in Figure 8. The strong electrostatic interactions between a carboxylate anion and water "ligands" result in "unstable" complexes which quickly lose their structural integrity during a molecular dynamics simulation. Bridging carboxylates clearly show directional binding to each Mn center which is lost if the metal is not attached to the ligands, while trigonal bipyramidal complexes of tripod donors lose their 3-fold symmetry.

$$E_\theta = k_2(\theta - \theta_0)^2 + k_3(\theta - \theta_0)^3 + k_4(\theta - \theta_0)^4 \qquad (1)$$

Having determined that a valence description is necessary, both oxygens of the carboxylate need to be connected to a metal center. A computational description of the desired flipping motion can then be obtained using an Mn−O−C angle potential function with multiple minima, an approach similar in spirit to that proposed by Allured et al.[34] for dealing with multiple L−M−L angles in, for example, planar Rh(I) complexes.

The simple function shown in equation 1 is already implemented in MOE but could easily be implemented in other MM codes. Setting $k_2 < 0$ and $k_4 > 0$ gives two minima (Figure 9). Judicious selection of force constants and θ_0, that is, the maximum of the energy curve, allows any desired minima and intervening barrier height to be obtained.

Remaining Force Field Parameters. In addition to parameters for the "organic" atoms, the force field is augmented with Morse functions for Mn−L bond stretching (although a similar result can be obtained from a quartic expansion) while the angular geometry at the metal is determined via a ligand−ligand repulsive term which depends on some inverse power of the distance between ligand donor atoms.[20] For bidentate carboxylate coordination, the intraligand O···O repulsion energy is explicitly removed.

The Merck Molecular FF (MMFF) force field[39–42] is used here because it has the richest selection of atom types. The O- and N-donors shown in Figure 10 were chosen as biologically most relevant. Although originally designed to include modeling of proteins, MMFF is seldom used for large biomolecules because its potential energy expression is more complex (and hence more compute intensive) than, say, AMBER[43] or CHARMM.[44] However, our previous study on siderophore complexes shows that the MMFF parameters can quickly be converted to any of the other FFs available in MOE.[45] Normally, this requires only a renaming of atom types. As will be described in a future publication, an equivalent treatment in AMBER has been developed for manganese metalloenzymes.

Although many previous MM[46,47] and LFMM[36,38,48–52] studies on small coordination complexes have omitted partial atomic charges, electrostatic interactions are important in biomolecular simulations.[53] The MMFF scheme includes a

(39) Halgren, T. A. *J. Comput. Chem.* **1996**, *17*, 490–519.
(40) Halgren, T. A. *J. Comput. Chem.* **1996**, *17*, 520–552.
(41) Halgren, T. A. *J. Comput. Chem.* **1996**, *17*, 553–586.
(42) Halgren, T. A.; Nachbar, R. B. *J. Comput. Chem.* **1996**, *17*, 587–615.
(43) Pearlman, D. A.; Case, D. A.; Caldwell, J. W.; Ross, W. S.; Cheatham, T. E.; Debolt, S.; Ferguson, D.; Seibel, G.; Kollman, P. *Comput. Phys. Commun.* **1995**, *91*, 1–41.
(44) Brooks, B. R.; Bruccoleri, R. E.; Olafson, B. D.; States, D. J.; Swaminathan, S.; Karplus, M. *J. Comput. Chem.* **1983**, *4*, 187–217.
(45) Lautru, S.; Deeth, R. J.; Bailey, L. M.; Challis, G. L. *Nat. Chem. Biol.* **2005**, *1*, 265–269.
(46) Comba, P.; Remenyi, R. *Coord. Chem. Rev.* **2003**, *238*, 9–20.
(47) Comba, P. *Coord. Chem. Rev.* **1999**, *186*, 81–98.
(48) Deeth, R. J.; Foulis, D. L.; Williams-Hubbard, B. J. *Dalton Trans.* **2003**, 3949–3955.
(49) Davies, I. W.; Deeth, R. J.; Larsen, R. D.; Reider, P. J. *Tett. Lett.* **1999**, *40*, 1233–1236.
(50) Deeth, R. J.; Paget, V. J. *J. Chem. Soc., Dalton Trans.* **1997**, 537–546.
(51) Burton, V. J.; Deeth, R. J.; Kemp, C. M.; Gilbert, P. J. *J. Am. Chem. Soc.* **1995**, *117*, 8407–8415.
(52) Burton, V. J.; Deeth, R. J. *J. Chem. Soc., Chem. Commun.* **1995**, 573–574.
(53) Warshel, A. *Annu. Rev. Biophys. Biomol. Struct.* **2003**, *32*, 425–443.

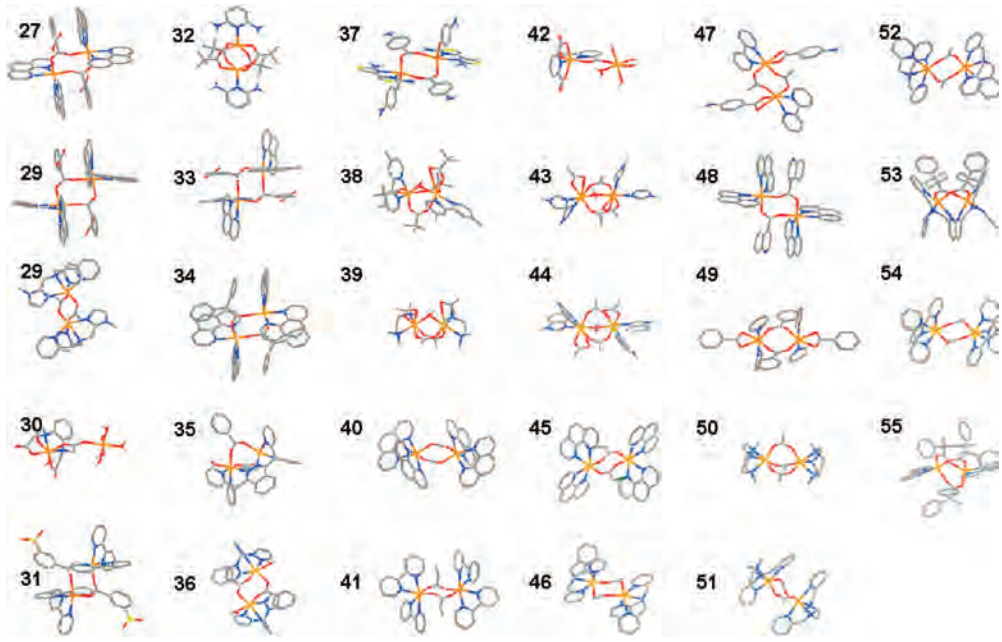

Figure 15. Line diagrams of dinuclear complexes based on X-ray structures. Numbering scheme as per Table 7.

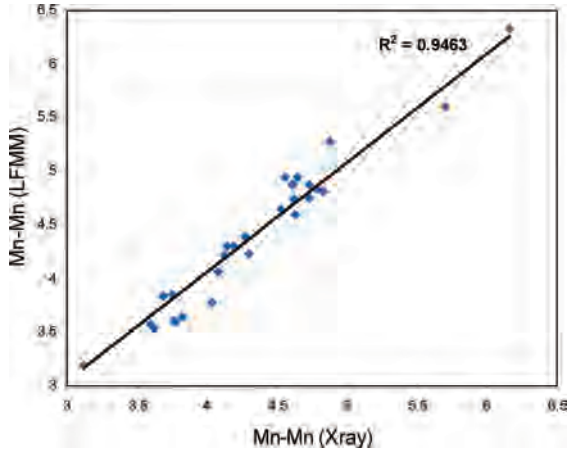

Figure 16. Plot of the correlation between X-ray structure and MM Mn−Mn separations.

relatively sophisticated method for assigning partial charges based on the bond charge increment (bci)[54] where the "base" partial charges of a pair of bonded atoms, A−B, are modified by the bci value for the A−B bond such that the change in charge on A is equal but opposite to that on B. The standard bci values for all bonded pairs in the ligand are retained with new bci values defined for the M−L pairs to model the M−L bond polarization and partially neutralize the metal charge. Because the metal is relatively "buried", the external electrostatic potential will be largely determined by the native FF charge scheme and the final results are not particularly sensitive to the precise M−L bci values.

DFT calculations on $[Mn(acetate)_2(OH_2)_4]$ suggest a net charge donation from a carboxylate group to Mn of about 0.16 electrons based on a Mulliken population analysis. While absolute Mulliken charges are not very reasonable, we are only interested in the change. The Mn+2-OX bci has therefore been set to 0.08. As a quick test of the significance of this value, the dipole moment for asymmetrically bound $[Mn(acetate)\ (OH_2)_5]^+$ was computed with and without the Mn−L bci. The dipole moment decreased from 7.8 to 7.5 Debye (the directions differ by less than 7 °) which is a relatively small change compared to the gas phase DFT value of 6.2 Debye. Of course, this small change does not mean that electrostatic effects are small, rather that the influence of the Mn−L bci on the overall charge distribution is relatively minor. The remaining M−L bci values are based on previous experience with other divalent metals and are listed in Table 4.

Twenty-six mononuclear and 29 dinuclear CSD hits survive the constraint of not exceeding a total coordination number of seven and of only comprising the donor atom types listed in Table 4. Morse function parameters plus ligand−ligand repulsion parameters (Table 5) were refined manually until an acceptable reproduction of experimental Mn−L bond lengths and heavy-atom superpositions was achieved (Tables 6 and 7).

The calculated structures for the mononuclear species (Figure 11) are in good agreement with those from single crystal X-ray diffraction studies with two-thirds of the bond lengths within 0.05 Å of experiment. The overall rmsd in M−L distances is 0.08 Å while individual rmsds are 0.05 Å or less for all atoms types except OX and OM (although there are only two examples of the latter). The larger deviations for Mn−OX are expected. In *all* cases, whatever binding mode is found in the crystallography is also predicted to be a stable local minimum. The training set has examples of both symmetric and asymmetric modes. The latter is favored by the angle bend term while symmetric coordination is favored by ligand−ligand repulsion. The balance between these competing FF terms enables both symmetric and asymmetric modes to be local minima.

(54) Bush, B. L.; Bayly, C. I.; Halgren, T. A. *J. Comput. Chem.* **1999**, *20*, 1495–1516.

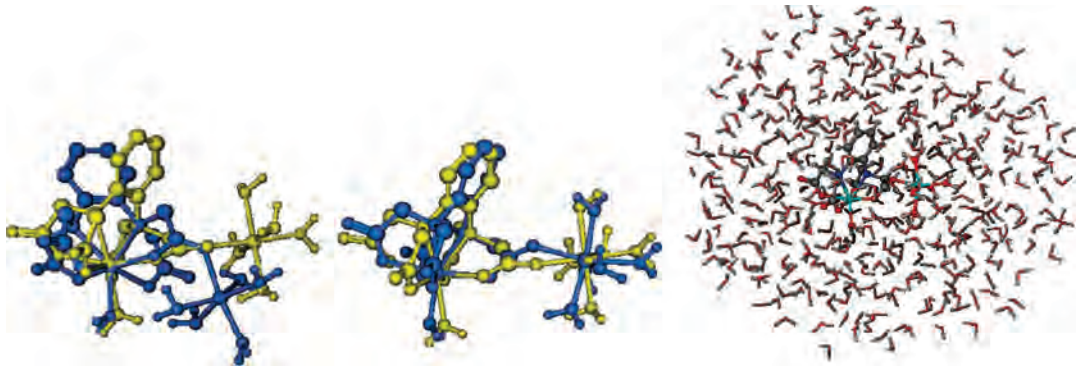

Figure 17. Comparison of X-ray (yellow) and calculated (blue) structures for DAJVOZ. Left: single-molecule optimization. Middle: optimization in the presence of 399 water molecules (water molecules hidden). Right: the solvated system.

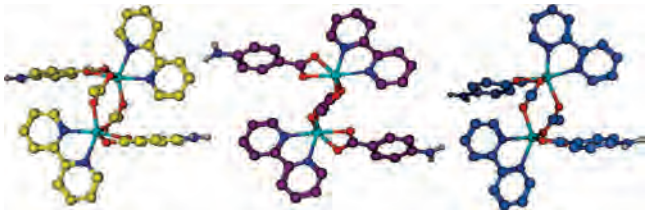

Figure 18. Relative orientation of bridging carboxylates in QANCIS. Left (yellow carbons): X-ray structure; middle (purple carbons): single molecule optimized geometry; right (blue carbons): optimized structure in water droplet (407 molecules, hidden).

The largest errors are in the longer Mn−O contacts in asymmetric bidentate coordination. The worst offender, pentaaqua-(2,4,5-trichlorophenoxyacetato)-manganese(II) (BIZYEO), has its long Mn−O distance reported to be 3.81 Å while MM gives 3.31 Å. If the long Mn+2-OX bonds are removed from the comparison, the rmsd across all mononuclear molecules falls to 0.06 Å which is only slightly larger than in other applications of the LFMM but, as discussed above, this is a consequence of requiring a single parameter set for several Mn-carboxylate binding modes each with a slightly different mean Mn−O distance.

Heavy-atom rmsd values are also good. The largest discrepancies are for systems like NAMKIW (Figure 12). Here, the whole carboxylate is displaced but the Mn−L rmsd remains acceptable (0.08 Å). However, in such cases, a heavy-atom superposition is not a good way to compare structures anyway and values more than about 1 are not very meaningful.

Six mononuclear systems display more-or-less symmetric bidentate coordination (DEFROW, HAZVAF, QUSVOP, ROCNUS, SUSXAF, XUQBIU, Figure 13). These are invariably related to polydentate donors which sometimes supply only four donor atoms (e.g., tripod ligands like tris(2-benzimidazolylmethyl)amine in DEFROW, ROCNUS, and SUSXAF) or are sometimes "restrained" such that a coordination site is relatively open (HAZVAF, QUSVOP, and XUQBIU). The X-ray structures are generally more asymmetric and Mn−O bonds longer than calculated suggesting that the current FF is slightly too "stiff" for the symmetric mode.

Note that a tripod donor does not guarantee the symmetric bidentate mode. SAFQEV has the same nitrogen-donor ligand as SUSXAF but an asymmetric binding mode. Of course, the calculations are started from the X-ray coordinates and so converge to the *nearest* local minimum. This may not be the lowest point on the theoretical potential energy (PE) surface.

Asymmetric bidentate coordination is often associated with an intramolecular hydrogen bond to an adjacent water ligand. An illustrative example is shown for aqua-(4-hydroxybenzoato-O)-bis(1,10-phenanthroline-N,N′)-manganese(II) (GAMFIK) in Figure 14. This motif is also common for metalloenzyme active sites. Note that despite the same $N_4(OH_2)(O_2CR)$ donor set, the planar arrangement of the 2,2′:6′,2″:6″,2‴-quaterpyridinato ligand in HAZVAF prevents the close approach of the water to the carboxylate and thus encourages symmetric bidentate binding of the latter (see Figure 13). For the other asymmetrically coordinated systems, the shorter Mn−O distance is often predicted to be slightly too long, that is, the FF is too "soft" for the asymmetric mode. The errors in the FF, that is, too stiff for symmetric and too soft for asymmetric binding result from requiring a single set of parameters to do both jobs. Similar behavior occurs for Cu(II) amine complexes where the calculated Cu−N distances for four-coordinate species tended to be a little short while those for six-coordinate species were, on average, a little long.[38]

The dimanganese complexes considered in this work are shown in Figure 15 and the structural comparison is presented in Table 7. The agreement between theory and experiment for both sets of complexes is comparable.

Two new features appear for dinuclear complexes. First, we have bridging water ligands which require an Mn−O−Mn angle bend term. A harmonic angle bending potential with a reference angle of 114 ° and a force constant of 20 kcal mol^{-1} $radian^2$ is suitable. Second, there is the Mn−Mn distance where the agreement between calculated and experimental Mn−Mn distances is excellent (Figure 16) with $R^2 = 0.95$. The only direct Mn−Mn interactions in the FF are the van der Waals and electrostatic terms. The former is negligible but the electrostatic energies are substantial. An approximate measure of electrostatic effects was obtained by reoptimizing selected complexes without electrostatics enabled. Although the Mn−Mn contribution will always be repulsive, the Mn−Mn distances actually fluctuate in both directions and by up to about 0.3 Å. We should therefore only trust the calculated Mn−Mn distance to about 0.3 Å.

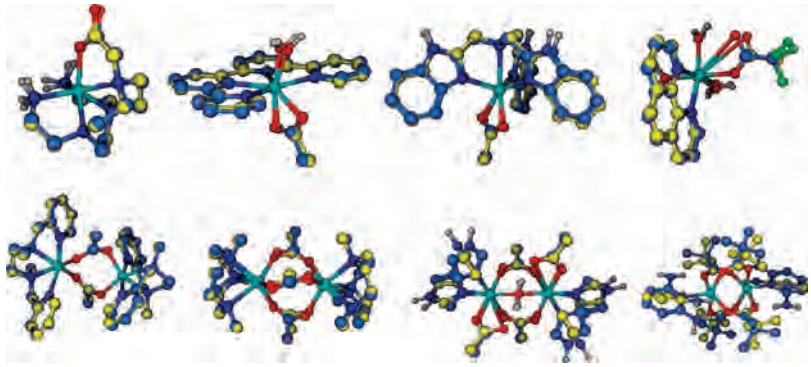

Figure 19. Overlay of X-ray (yellow carbons) and MM calculated (blue carbons) structures for selected mono- and dinuclear complexes.

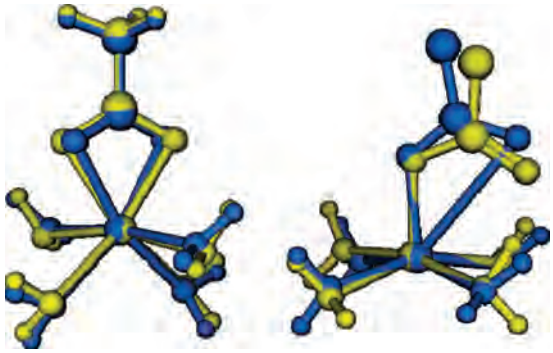

Figure 20. Overlays of MM (blue) and DFT (yellow) structures for symmetrical (left) and asymmetrical (right) bidentate acetate coordination in $[Mn(acetate)(OH_2)_4]^+$.

More detailed examination of the dinuclear structures reveals other discrepancies. The X-ray crystal structure of DAJVOZ orients the "pendant" $\{Mn(OH_2)_5\}$ moiety away from the rest of the complex such that the bridging C−O−Mn angle is 140 °. However, optimization causes this group to "fold" in upon the rest of the complex as shown on the left of Figure 17. This is clearly an intramolecular electrostatic interaction which is an artifact of "single-molecule" optimization. In the solid state, such interactions compete with intermolecular ones.

Within the theoretical model, such "anomalies" can be removed either by disabling the electrostatic interactions or, more sensibly perhaps, by improving the molecular model. The simplest way to include environmental effects is to add explicit solvent. Consequently, the complex was placed in a droplet of water molecules 10 Å thick (399 waters, Figure 17, right) and the whole system reminimized. The middle part of Figure 17 (where the water molecules have been hidden) now shows how the $\{Mn(OH_2)_5\}$ unit remains more-or-less in its crystallographic position. The calculated data in Table 7 actually refer to this solvated system.

Another example of condensed-phase effects is the relative orientation of the two bridging acetates in QANCIS. In the X-ray structure (Figure 18, left), the bridging groups lie in different but parallel planes while in the single-molecule optimized structure (Figure 18, middle) both bridging groups are in the same plane. Reoptimizing after solvating the complex in a water droplet 10 Å thick (407 solvent molecules) retains the X-ray configuration albeit at the expense of a 0.5 Å increase in the Mn−Mn contact.

On balance, the FF derived from a reasonably large and diverse training set gives accurate structures (Figure 19). Any significant discrepancies suggest "interesting" behavior due to environmental effects. In such cases, explicit solvation improves the computed results. For the others, explicit solvent does not generally alter the structure significantly (vide infra).

Energetics. Experimental measures of relative energies are not available. Hence, we are forced to use a "better" theoretical model to validate the MM energies. The obvious choice, especially for TM systems, is DFT.[55] While DFT is by no means perfect and different functionals may struggle to provide an accurate description of, say, bond dissociation energies,[56] spin-state energy differences,[57] or transition states,[58] significant progress is being made. Moreover, in the present context, we only require DFT to provide good structures and reasonable estimates of the energy differences between very similar isomeric species. As a first step, then, we consider, symmetric and asymmetric carboxylate binding in $[Mn(acetate)(OH_2)_n]^{2+}$, $n = 4, 5$. The structures present no difficulties[59] and are not especially sensitive to the (gradient corrected) functional so BP86 has been used with a DZP basis. We can anticipate M−L bond lengths accurate to about 0.02 Å. However, the energies can be more sensitive to the functional so we also consider PW91 and B3LYP and use larger TZP basis sets. As described below, the energy differences appear accurate to a few tenths of a kcal mol^{-1}.

For $n = 5$, we expect an asymmetric bidentate mode with intramolecular H-bonding as in molecule **2** of Figure 11. Both DFT/BP86 and MM give local minima with the long oxygen interacting via H-bonds with two equatorial water ligands. By repositioning the acetate for symmetrical binding, the MM optimization converges to a new minimum which is 2.2 kcal mol^{-1} higher. Using this structure as the starting point for a BP86 optimization also generates a local minimum (all frequencies positive) which is 2.4 kcal mol^{-1} higher than for the asymmetric bidentate mode. PW91 and B3LYP give

(55) Ziegler, T.; Autschbach, J. *Chem. Rev.* **2005**, *105*, 2695–2722.
(56) Schultz, N. E.; Zhao, Y.; Truhlar, D. G. *J. Phys. Chem. A* **2005**, *109*, 11127–11143.
(57) Ghosh, A. *J. Biol. Inorg. Chem.* **2006**, *11*, 712–724.
(58) Patchkovskii, S.; Ziegler, T. *J. Chem. Phys.* **2002**, *116*, 7806–7813.
(59) Hocking, R. K.; Deeth, R. J.; Hambley, T. W. *Inorg. Chem.* **2007**, *46*, 8238–8244.

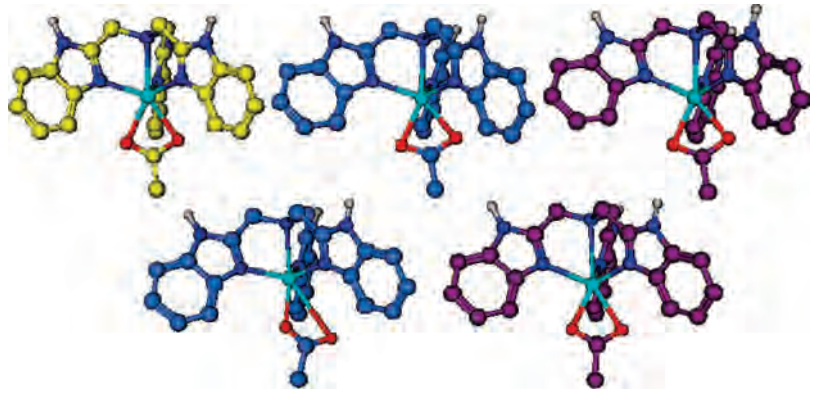

Figure 21. X-ray (yellow), MM (blue), and DFT (purple) structures for ROCNUS. Top row: symmetric bidentate. Bottom row: asymmetric bidentate.

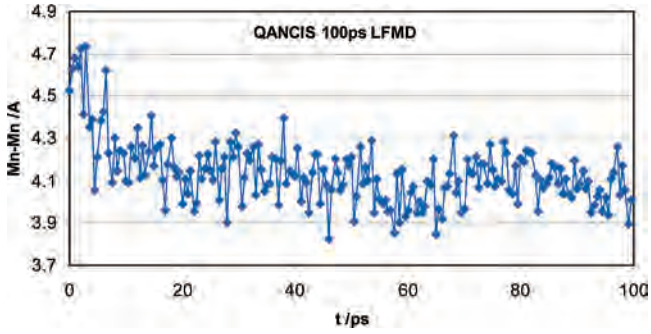

Figure 22. Mn−Mn distance from 100 ps MD run on QANCIS (see Figure 18).

similar differences of 2.2 and 1.6 kcal mol^{-1}, respectively, confirming that the MM energetic balance between asymmetric and symmetric coordination appears to be good.

[Mn(acetate)$(OH_2)_4$]$^{2+}$ is expected to favor symmetric coordination and indeed MM places the symmetrically bound system about 11 kcal mol^{-1} lower than for the asymmetric mode. However, although DFT generates the same structure as MM (Figure 20), it predicts a much smaller difference (the symmetric binding mode is only 0.5 kcal mol^{-1} lower than asymmetric).

The big difference between MM and DFT energies for [Mn(acetate)$(OH_2)_4$]$^{+}$ is troubling. However, this system, while at first sight an acceptable theoretical model for DFT is a rather "exotic" test case for MM because the FF parameters were based on actual coordinatively saturated complexes. This is especially the case for the ligand−ligand repulsion parameters. The problem could be corrected by including low-coordination-number complexes in the training set but because such species would be hypothetical (for Mn(II)) and not experimentally relevant, modifying the ligand−ligand repulsion does not seem worthwhile. Instead, a better test is use a "real" molecule such as acetato-(tris(2-benzimidazolylmethyl)amine)-manganese(II) (ROCNUS) (Figure 21).

The X-ray crystal structure gives a symmetric bidentate mode (Mn−O 2.24 and 2.29 Å) and the MM- and DFT-optimized structures are in good agreement (Mn−O 2.19 and 2.21 for MM and 2.17 and 2.18 Å for DFT). An asymmetric binding mode can be found on the MM potential energy surface (Mn−O 2.13 and 3.28 Å) which was used as the starting point for a DFT optimization which retains an element of asymmetry but somewhat reduced compared to MM (the Mn−O distances are 2.11 and 2.32 Å). MM places the symmetric structure 2.1 kcal mol^{-1} lower than asymmetric while the DFT energy differences are 1.4 kcal mol^{-1} (BP86), 1.8 (PW91), and 1.9 (B3LYP). While smaller, they are at least in the correct sense and given that the asymmetric structures are different, the agreement restores our confidence in the MM energies. Note also that the MM structure gives significantly shorter Mn−O distances than experiment but this does not appear to have significantly affected the relative energies. However, these calculations also demonstrate the fine balance between binding modes with asymmetric favored by a few kcal mol^{-1} for higher coordination numbers and symmetric favored by a few kcal mol^{-1} for lower coordination numbers. Environmental factors could be significant.

An important environmental factor is solvation. As discussed above, MM optimization in the presence of explicit solvent was used to "cure" some discrepancies. However, given that a simple optimization locates the nearest local minimum, and that the calculation was started from the X-ray structure, the solvent may be accidentally reinforcing the starting point.

For QANCIS (Figure 18), solvation corrected the relative orientation of the bridging carboxylate planes but increased the Mn−Mn distance by 0.5 Å. Molecular dynamics (MD, MD including ligand field effects has recently been implemented in DommiMOE as will be reported in due course) reveals the latter is in fact an artifact of a less-than-ideal configuration of solvent molecules. Within 17 ps of a 100 ps NVT MD run, the Mn−Mn distance relaxes from the long 4.5 Å seen in the "static" optimization to an average of 4.08 ± 0.10 Å over the final 50 ps (Figure 22) which is identical to the X-ray value. Moreover, the two carboxylates are not coplanar, just as in the solid state.

Another interesting feature of carboxylate coordination is whether the ligand can "flip", that is, interchange the long and short Mn−O bonds in asymmetric bidentate mode. The alternative to flipping is a rotation by 180 °. For a simple system like [Mn(acetate)$(OH_2)_5$]$^{+}$, MD clearly shows that with the current FF, rotation is the preferred mechanism. The projection of the plane of the axial carboxylate onto the equatorial plane bisects two Mn−OH_2 bonds such that relative to a given equatorial water ligand, the C−O−Mn−O(aq) dihedral is either 45, 135, −135, or −45 °. Figure 23 (top)

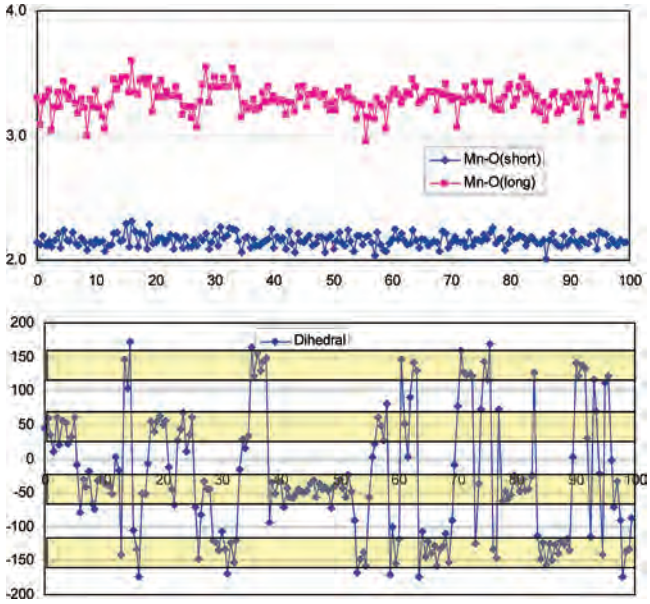

Figure 23. Structural results from 100 ps LFMD simulation of [Mn(acetate)$(OH_2)_5]^+$. Top: Mn−O distances (Å). Bottom: Mn−O−C−O dihedral (°). The yellow banding indicates the four stable locations of the carboxylate relative to the equatorial $Mn(OH_2)_4$ plane.

shows how the Mn−O(short) and Mn−O(long) bonds retain their relative lengths while Figure 23 (bottom) shows how the plane of the carboxylate makes 90 ° jumps about every 5 ps.

To explore flipping in "real" complexes, MD simulations for tripod donor systems were carried out but despite having different binding modes in the X-ray structures, they all collapse to symmetric binding during MD and no flipping can be observed. The asymmetric mode for complexes like SUSXAF is only meta stable.

The ability to carry out MD simulations is a powerful tool for modeling TM systems. However, without special procedures, MD cannot easily overcome large conformational energy barriers spontaneously and the simulation may become trapped in a localized region of phase space. In contrast, stochastic methods offer an improved chance not only of locating the overall lowest-energy structure but also other local minima at higher energies.

To deal with metal complexes, we have modified the MOE stochastic search algorithm, which is similar to the random incremental pulse search method described by Ferguson and Raber.[60] Starting conformations are generated by adding random increments to all rotatable bonds, excluding those which involve the metal and its nearest neighbors. An initial fast optimization is carried out (lower van der Waals cutoff of 4 Å instead of 8 Å, no electrostatics or stretch−bend terms) until the gradient norm is less than 5. A full MM optimization follows until the gradient norm is less than 0.5 then the current energy is tested against the lowest obtained so far and if it is within a certain threshold, a further full MM optimization follows down to a gradient norm threshold

(60) Ferguson, D. M.; Raber, D. J. *J. Am. Chem. Soc.* **1989**, *111*, 4371–4378.

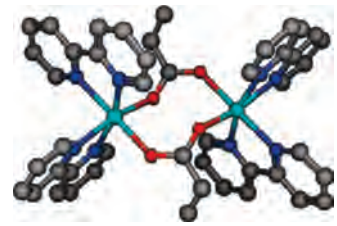

Figure 24. X-ray structure of NEMCAJ (right) with approximately syn-anti bridges. Hydrogen atoms omitted for clarity.

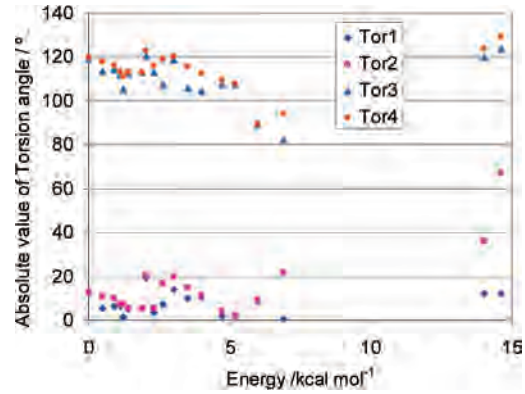

Figure 25. Relationship between the absolute values of the four possible Mn−O−C−O torsion angles, Tor1 through Tor4, and the conformational energy for NEMCAJ.

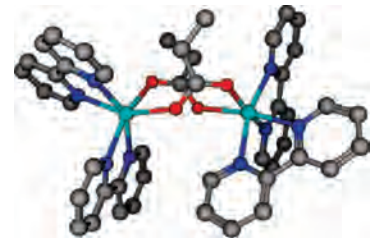

Figure 26. High-energy form of NEMCAJ from stochastic search.

of 0.02. The structure is retained if the final energy is lower than or within a preset threshold (usually 10 kcal mol^{-1}) of the current "best", otherwise it is discarded.

The starting conformations generally have severely distorted metal coordination which facilitates a thorough examination of all possible coordination geometries. To illustrate the usefulness of stochastic searching, we consider the dinuclear complex NEMCAJ which has approximately syn-anti bridges with torsions of 12 and 120 ° as compared to the ideal Mn−O−C−O torsion angles for syn and anti of 0 and 180°, respectively.

A 1000 step stochastic search leads to a number of low-energy conformations of gradually increasing energy (up to about 7 kcal mol^{-1} above the minimum) but without any substantial alteration of the syn-anti arrangement of the carboxylates (Figure 25). There follows a jump of about 7 kcal mol^{-1} but although the structure is more distorted, it does not correspond to a transition to syn-syn mode. Instead, both bridges end up "cis" to each other in terms of the orientation of the carboxylate substituents (Figure 26) as opposed to the usual, and much lower energy "trans" arrangement shown in Figure 24. This type of bridging mode is found at the active site of MetAP (PDB code 2GU7, see

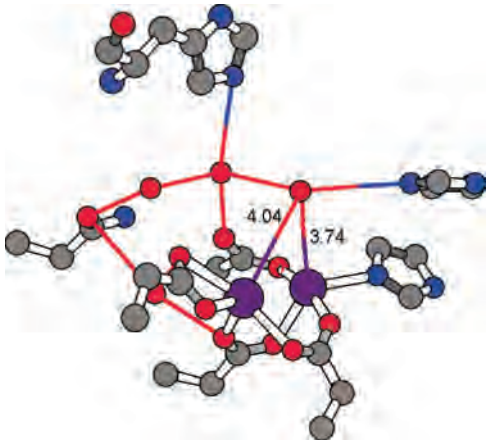

Figure 27. Active site detail for methionine aminopeptidase I (PDB code 2GU7) including solvent waters. Hydrogens and backbone atoms omitted. Narrow lines represent nominal H-bonds.

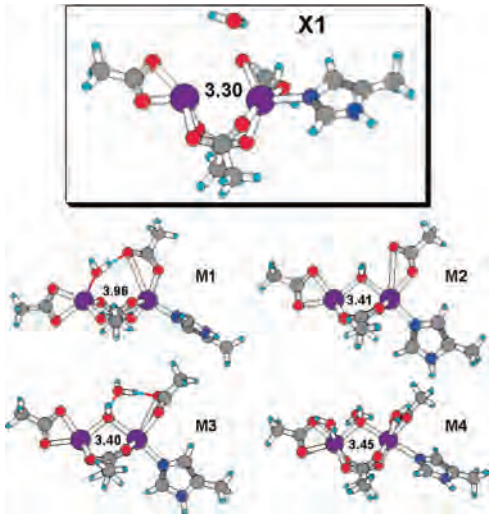

Figure 28. MetAP1 models viewed down the vector joining the two bridging carboxylate carbon atoms: X-ray structure (X1) and various MM models (see text). Mn−Mn distance shown in Å.

Figures 2 and 28) but the MM result suggests it should not be stable.

The difference is that, in the protein, there is also a bridging water ligand. Significantly, although several solvent water molecules are reported in the Protein Data Bank (PDB) structure (Figure 27), the nearest candidate is more than 3.7 Å from either Mn center. Thus, and as a prelude to a full report on the application of MM to manganese-containing proteins, we can use MM on active site models to explore the details of the metal coordination.

A series of models were optimized and compared to the "in-crystal" model, X1.

The first model, M1, is the MM-optimized version of X1. There is a substantial relaxation with M1 having a much longer Mn−Mn distance than in the PDB structure (3.96 Å in M1 versus 3.3 Å in X1). As expected, explicitly coordinating the water ligand in a bridging position (M2) dramatically improves the Mn−Mn distance and generally improves the picture around the left-hand Mn. However, the geometry around the right-hand Mn is different. In particular, MM gives the Mn−N bond trans to the Mn−O of the bridging water while the X-ray structure positions it parallel to the Mn−Mn vector. The asymmetric-bidentate carboxylate has moved through about 90° from approximately perpendicular to the Mn−O(H_2)−Mn plane to more or less parallel. Also, MM tends to eclipse the CO_2 moieties of the bridging carboxylates while experimentally, they appear to be slightly twisted.

Some of the remaining differences can be lessened or removed by adding further water molecules to the theoretical model. Thus, the asymmetric bidentate carboxylate can be encouraged to move backward via hydrogen bonding to an additional water molecule (M3) while binding an extra water molecule to the right-hand Mn center causes the bridging carboxylates to twist (M4). Thus, the (apparently incomplete) X-ray diffraction data provide clues which we can exploit via MM calculations to help determine what might be missing. Of course, the optimized structure of the model systems is still not identical to that reported experimentally. This could be due to deficiencies in the experiment and/or the calculations. For the latter, there might be substantial "entatic state" [61] effects exerted by the protein backbone. This requires MM and MD calculations on complete systems which, as intimated above, will be the subject of a future communication.

Conclusions

The first valence force field approach capable of modeling symmetric bidentate, asymmetric bidentate and bridging carboxylates with a single parameter set has been developed and applied to mono- and dinuclear Mn(II) complexes. In addition to carboxylates, amine, pyridyl, imidazolyl, pyrazolyl, and water ligands are considered. The parameters are based on the Merck molecular force field, although conversion to AMBER or CHARMM would be straightforward, augmented by Morse function expressions for Mn−L bonding together with explicit ligand−ligand repulsion terms in lieu of an L−M−L angle-bending potential. Both features are available in our ligand field molecular mechanics extension of the molecular operating environment (MOE). However, since by definition, the ligand field stabilization energy for high spin d^5 species is zero, an equivalent scheme can be implemented purely within MOE (or any other MM package) by setting the L−Mn−L angle-bending force constants to zero, adding new code for ligand−ligand repulsions, and mapping the Morse functions onto the existing bond-length potential expression. Partial atomic charges were implemented using the MMFF bond charge increment scheme.

A training set of 55 crystallographically characterized complexes was used. Significant directionality is found for Mn−carboxylate interactions such that a "bare" Mn^{2+} cation approach gives poor structures, especially for multimetal systems. A bonded, valence FF is required. The crucial feature for treating multiple carboxylate binding modes is a multiterm Mn−O−C angle bend potential. A quadratic term with a negative force constant plus a quartic term with a

(61) Vallee, B. L.; Williams, R. J. P. *Proc. Natl. Acad. Sci. U.S.A.* **1968**, *59*, 498–505.

positive force constants gives a double minimum potential which, in combination with the other FF terms, provides a balanced description of both asymmetric and symmetric bidentate coordination. In principle, this approach can be applied not only to other metals but to other ligands like nitrate and sulfate which also have multiple binding modes.

The calculated structures are in good agreement with experiment. In every case, the model faithfully reproduces the observed carboxylate binding mode. Moreover, although the overall M−L bond length rmsd between MM and X-ray crystal structures of 0.08 Å is relatively large, the experimental uncertainties necessary to cover the entire training are also quite large. However, this does not have an adverse affect on the relative energies as judged by comparison to DFT. This behavior is consistent with QM studies which also show that the energy is not especially sensitive to structure.

The MM-based model is computationally efficient and thus facilitates modeling the dynamical behavior of metal complexes. MD simulations show that rotation of an asymmetric bidentate carboxylate is generally favored over "flipping" while the asymmetric mode in complexes of tripod donors is only meta stable.

For dinuclear complexes, the Mn−Mn distance is reproduced to within about 0.3 Å, including those cases with bridging water ligands for which an additional Mn−O−Mn energy term is required. Preliminary MM calculations on models for the dimanganese active site of methionine aminopeptidase illustrate how incomplete and/or inaccurate models based on X-ray diffraction can be refined and improved using MM. Further detailed applications of MM to Mn-containing enzymes will be the subject of a future communication.

Acknowledgment. The author acknowledges access to the CSD via the EPSRC's Chemical Database Service, the financial support of Chemical Computing Group and GlaxoSmithKline and the many useful discussions with Drs. Mike Hann and Pam Thomas.

Supporting Information Available: Form of the MOE potential energy; Table S1: CSD refcodes for mononuclear Mn(II) complexes; Table S2: CSD refcodes for dinuclear, bridging-carboxylate Mn(II) complexes; Table S3: Full bibliographic and chemical data for mononuclear complexes; Table S4: Full bibliographic and chemical data for dinuclear complexes (PDF). This material is available free of charge via the Internet at http://pubs.acs.org.

IC800313S